PHYSICAL REVIEW B **92**, 161114(R) (2015)

Magnetism, superconductivity, and quantum criticality in the multisite cerium heavy-fermion compound Ce_3PtIn_{11}

J. Prokleška, M. Kratochvílová, K. Uhlířová, V. Sechovský, and J. Custers
Charles University in Prague, Faculty of Mathematics and Physics, Ke Karlovu 5, 121 16 Prague 2, Czech Republic
(Received 9 July 2015; revised manuscript received 7 September 2015; published 22 October 2015)

The properties of the heavy-fermion superconductor Ce_3PtIn_{11} are investigated by thermodynamic and transport measurements at ambient and under hydrostatic pressure. At ambient pressure the compound exhibits two successive magnetic transitions at $T_1 \simeq 2.2$ K and $T_N \simeq 2$ K into antiferromagnetically ordered states and enters into a heavy-fermion superconducting phase below $T_c \simeq 0.32$ K. The coexistence of long-range magnetic order and superconductivity is discussed in the context of the existence of the two crystallographically inequivalent Ce sites in the unit cell of Ce_3PtIn_{11}. The experimental data allow us to construct the pressure-temperature phase diagram.

DOI: 10.1103/PhysRevB.92.161114 PACS number(s): 75.30.Mb, 74.25.Dw, 74.40.Kb, 75.30.Kz

In several classes of strongly correlated electron systems such as heavy-fermion (HF) materials, superconductivity emerges in the vicinity of a quantum critical point (QCP). The general view is that critical fluctuations associated with the order parameter of the phase transition at the critical point enhance the interaction between electrons in a similar way phonons do in conventional superconductors leading to superconductivity (SC) [1]. In fact superconductivity has been reported in numerous HF materials to emerge at the border of a magnetically ordered state and a paramagnetic state indicative of magnetically mediated SC [2,3].

The majority of the cerium HF compounds studied to date have one crystallographic site for the cerium ions. In compounds with two or more inequivalent sites, the different local environment of corresponding Ce ions results in different interaction of the Ce $4f$ states with the surrounding ligand and conduction states. This in turn will lead to different Kondo coupling strength. Consequently, a variety of new and complex phenomena might be expected in these multisite cerium compounds where the ground state is characterized by a coexistence of different electronic and magnetic states on a microscopic scale. Such is well illustrated in cubic $Ce_3Pd_{20}Si_6$ where one Ce site exhibits dipolar ($T_N \approx 0.3$ K) and the second site quadrupolar antiferromagnetic (AFM) order ($T_Q \approx 0.5$ K) [4–6]. The compound arouses special attention displaying pronounced non-Fermi liquid behavior and a field-induced QCP ($T_N \to 0$ for $B_c \approx 0.9$ T) of Kondo breakdown type which separates two different ordered phases [7]. Theoretically, little has been investigated on the behavior of multiple distinct Kondo lattices. Benlagra and co-workers discussed a Kondo lattice comprising two local-moment sublattices, coupled with different Kondo couplings (T_{K1} and T_{K2}) to conduction electrons, factually describing a compound with two inequivalent, for instance, Ce sites [8]. Particularly interesting is the situation of partial screening ($T_{K1} > T > T_{K2}$), where one sublattice is in a non-magnetic Kondo screened state forming heavy quasiparticles, while the second sublattice still carries local magnetic moments. Here, any magnetic long-range ordered (LRO) state, hence, will manifest characteristics of a weakly polarized HF phase coexisting with properties of typical local-moment magnetism. Such has been reported for Ce_7Ni_3 which possesses even three inequivalent Ce sites [9]. In this context one may speculate that under certain conditions the HF sublattice becomes superconducting while the second sublattice remains magnetically ordered.

Here we introduce a new multisite cerium HF compound, Ce_3PtIn_{11}. It belongs to the $Ce_nT_mIn_{3n+2m}$ class of materials which comprises a numerous amount of compounds including $CeCoIn_5$, $CeRhIn_5$, and Ce_2RhIn_8 [10,11]. The crystal structure of Ce_3PtIn_{11} is like that of Ce_3PdIn_{11} (space group $P4/mmm$) when replacing Pd by Pt [12]. The lattice parameters at room temperature are $a = 4.6874(4)$ Å and $c = 16.8422(12)$ Å. The three Ce ions in the Ce_3PtIn_{11} unit cell are distributed within two crystallographically inequivalent sites. Two Ce ions reside in the Ce1 position (Wyckoff $2g$ place, D_{4h} symmetry) which are surrounded by ligands similar to the Ce ions in Ce_2PtIn_8 [12]. The Ce2 site (Wyckoff $1a$, C_{4v} symmetry) is occupied by 1 Ce ion. The ion experiences a $CeIn_3$-like environment. At ambient pressure and in the absence of magnetic field the material shows remarkable properties: Ce_3PtIn_{11} undergoes two successive magnetic transitions at $T_1 \simeq 2.2$ K and $T_N \simeq 2$ K into AFM states [12] and becomes superconducting below $T_c \simeq 0.32$ K (this paper). We, thus, consider Ce_3PtIn_{11} as a promising candidate for (i) studying the complex behavior of two different mutually interacting Ce sites and (ii) examining the interplay of SC and magnetism.

Single crystals of Ce_3PtIn_{11} used in the present study were grown out of excess In flux. Details about crystal growth and characterization can be found in Ref. [12]. The magnetic susceptibility in the temperature range from 1.8 to 300 K was determined utilizing a commercial MPMS 7 T SQUID magnetometer from Quantum Design (QD) with an applied field of 0.1 T. For the low temperature experiments the sample was mounted to a Leiden Cryogenics MCK72 dilution refrigerator. A maximum field of 9 T can be applied. Measurements to higher temperatures were performed in a QD PPMS 9 T. Electrical resistivity experiments were conducted by standard four point ac technique. The relaxation method was applied to determine the specific heat (temperature range of $0.15 < T < 30$ K). We used a QD dilution refrigerator heat capacity puck for the specific heat measurements in the MCK72. To apply hydrostatic pressure up to about 2.5 GPa the sample was loaded into a double cylinder CuBe/NiCrAl

pressure cell. Daphne 7373 oil was used as a pressure medium. All stated pressures are at low temperatures.

Before presenting the low temperature properties of Ce_3PtIn_{11}, we briefly summarize the behavior above 3 K (not shown). The electrical resistivity ρ is similar in magnitude and behavior to the other $Ce_nT_mIn_{3n+2m}$ compounds: At 300 K the c-axis resistivity equals 60 $\mu\Omega$ cm, approximately 1.5 times larger than ρ in the basal plane. Upon lowering the temperature ρ shows a weak temperature dependence with $d\rho/dT > 0$. Below ≈30 K the resistivity drops rapidly marking the crossover from incoherent Kondo scattering at high temperatures to the formation of heavy-electron Bloch states at low temperatures. The susceptibility as a function of temperature, $\chi(T)$, has been measured in a magnetic field applied perpendicular ($\perp c$) and along ($\| c$) the crystallographic c axis and appears to be weakly anisotropic with a ratio $\chi^{\| c}/\chi^{\perp c} \approx 1.25$ at 3 K. Above 150 K $\chi(T)$ follows Curie-Weiss law with a value of the effective moment of $\mu_{\rm eff} = 2.60\,\mu_B$/Ce for both directions, in good agreement with the expected Hund's rule value for a free Ce^{3+} ion ($2.54\mu_B$). The obtained Weiss temperatures from fitting yield $\theta_p^{\perp c} = -64$ K and $\theta_p^{\| c} = -42$ K.

Figure 1 displays the ambient pressure thermodynamic and transport properties of Ce_3PtIn_{11} at low temperatures. The results are plotted in the same temperature interval (0–3 K) one below the other to compare the associated anomalies and to complement the methods among each other. The inset in Fig. 1(a) shows the low-T susceptibility $\chi^{\| c}$ in a wider temperature range. A broad structure with a maximum at $T_{\chi^m} = 2.8$ K is seen which we attribute to the presence of short-range AFM correlations [13]. At slightly lower temperatures these correlations lead to AFM ordering (AFM1) manifested by a sharp decline in $\chi(T)$ at T_1 [Fig. 1(a)]. The second AFM transition at $T_N \simeq 2.0$ K appears as a weak bumplike structure in the 0.1 T data. The zero field electronic part of the specific heat C_{el}/T displayed in Fig. 1(b) has been determined by subtracting the lattice term β of the Debye fit ($C/T = \gamma_0 + \beta T^2$; fit interval $10 < T < 30$ K) from the total specific heat, i.e., $C_{el}/T = C/T - \beta T^2$. The fit yields a Sommerfeld coefficient $\gamma_0 = 0.52$ J/(mol K^2) and $\beta = 5.58$ mJ/(mol K^4). The latter value transforms into a Debye temperature of $\Theta_D = 174$ K. The contribution arising from the crystal electric field can be neglected for these low temperatures. The magnetic transitions are clearly visible as pronounced jumps in C_{el}/T. The higher temperature transition is characterized by a shallow kink in the temperature dependence of the electrical resistivity only. In contrast, the transition at the lower temperature is manifested as a steep decrease of ρ. It strongly mimics the behavior of $\rho(T)$ for $CeRhIn_5$ for $T < T_N = 3.8$ K [14]. We define the midpoint of the C_{el}/T jumps as transition temperatures yielding $T_1 \simeq 2.2$ K and $T_N \simeq 2$ K, respectively. These values coincide reasonably with the features in $\chi(T)$ and $\rho(T)$ (dashed lines in Fig. 1). The most intriguing feature in C_{el}/T is observed around 0.35 K. It signals the transition into a superconducting phase as corroborated from resistivity data. The jump is slightly broadened, and hence we define the transition temperature at the midpoint of the jump height becoming $T_c \simeq 0.32$ K. To estimate the normal state specific heat coefficient γ_n we extrapolated the low-T tail of the AFM transition towards $T = 0$ [red dashed line in Fig. 1(b)] employing a second-order mean-field type

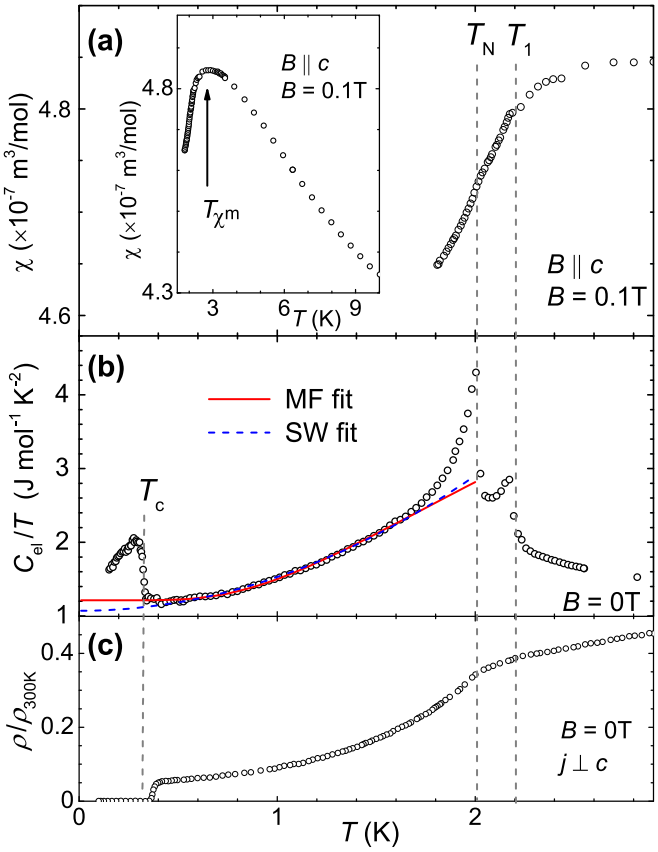

FIG. 1. (Color online) Overview of low temperature properties of Ce_3PtIn_{11} for $T < 3$ K. (a) Temperature dependence of χ vs T in field $B = 0.1$ T applied $\| c$ axis. Inset shows the data up to 10 K. The arrow indicates the maximum in $\chi(T)$. (b) Electronic part of the specific heat C_{el}/T as a function of T in zero field. The red solid and blue dashed lines are, respectively, a mean-field (MF) and spin wave (SW) fit of $T < 0.8T_N$ towards $T = 0$ (see text). (c) Resistivity normalized to its room temperature value in $B = 0$ T and $j \perp c$.

expression, $C_{el}/T = \gamma_n + A\exp^{-\Delta_{AFM}/T}$ [15]. The resulting parameters are $\gamma_n = 1.21$ J/(mol K^2), $A = 8.97$ J/(mol K^2), and $\Delta_{AFM} = 3.44$ K (fit interval $0.44 < T < 1.6$ K). As shown, a fit $C_{el}/T \propto T^2$ (AFM spin wave [16]) describes the data in the same interval with a similar quality but with a reduction in γ_n by ≈10%. Using above parameters allows calculation of the parameter $\Delta C/(\gamma_n T_c) \approx 0.7$ that is roughly half of the expected value from BCS theory. However, we implicitly assumed here that the electrons in the conduction band participating in SC originate in equal measures from the two Ce sites. This assumption might not be correct as discussed later on. The magnetic entropy, $S_{mag} = \int_0^T C_{el}/T\,dT$, with the mean-field expression replacing the SC part, is presented in Fig. 2.

To provide additional information about the superconducting state we determined the upper critical field B_{c2} using data depicted in Fig. 3. The midpoint of the jump defines T_c, which is shown in Fig. 3(b). The expression for orbital limited superconductivity, $B_{c2} = B_{c2}^{orb}(T = 0)[1 - (T/T_c)^2]$, describes the data reasonably well with $B_{c2}^{orb}(0) = 1.4$ T and an initial slope $-dB_{c2}/dT|_{T=Tc} = 7.24$ T/K. Because $B_{c2}^{orb} \propto$

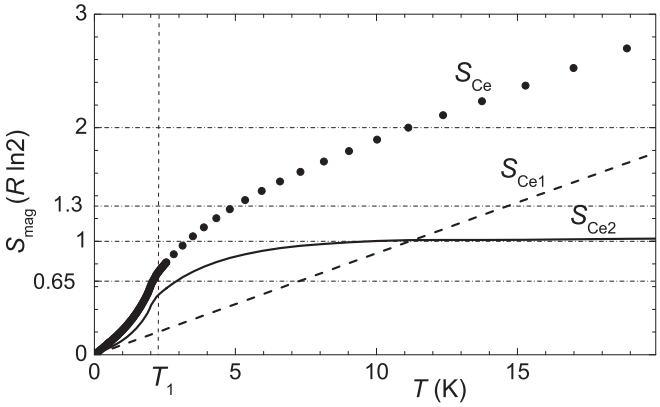

FIG. 2. The magnetic entropy S_{mag} associated with C_{el}/T (S_{Ce}; symbols), the Ce1 sublattice (S_{Ce1}; dashed line) and the Ce2 sublattice (S_{Ce2}; solid line) as discussed in the text.

$(m^*)^2 T_c^2$ it is evident that heavy quasiparticles, mass m^*, are involved in Cooper pairing.

In the following we investigate the influence of hydrostatic pressure on the magnetic and SC transitions by means of ac calorimetry and resistance measurements [Figs. 4(a) and 4(b)]. The p-T phase diagram in Fig. 5 collects the pressure results. We observe that the magnetic transition temperatures decrease with increasing pressure and become absent once they intersect with superconductivity at $p \simeq 1.1$ GPa. For pressures between 1.1 and 1.6 GPa, superconductivity evolves out of a non-Fermi liquid state which is characterized by an almost T-linear resistivity from T_c ($\simeq$0.7 K) to temperatures even higher than $T > 5$ K. The maximum in T_c points to the position of the magnetic QCP being located at $\approx$1.3 GPa [2,17]. A fit to $R(T)$ at p_c gives $R = R_0 + AT^n$ with $n = 0.90 \pm 0.05$ for $0.8 \leqslant T \leqslant 7$ K [inset Fig. 4(b)]. A similar exponent has also been reported above T_c for $CeRhIn_5$ [18] and Ce_2RhIn_8 [19] near their critical pressures raising speculation that also in Ce_3PtIn_{11} the quantum criticality is local. However, within

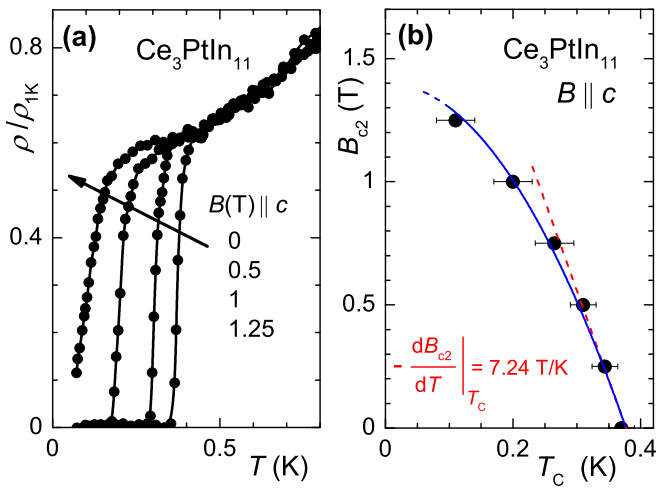

FIG. 3. (Color online) Selection of low temperature $\rho(T)$ runs in applied field (a) and the derived phase diagram for B_{c2} (b). The red dashed line depicts the slope in the vicinity $B_{c2} \to 0$ T.

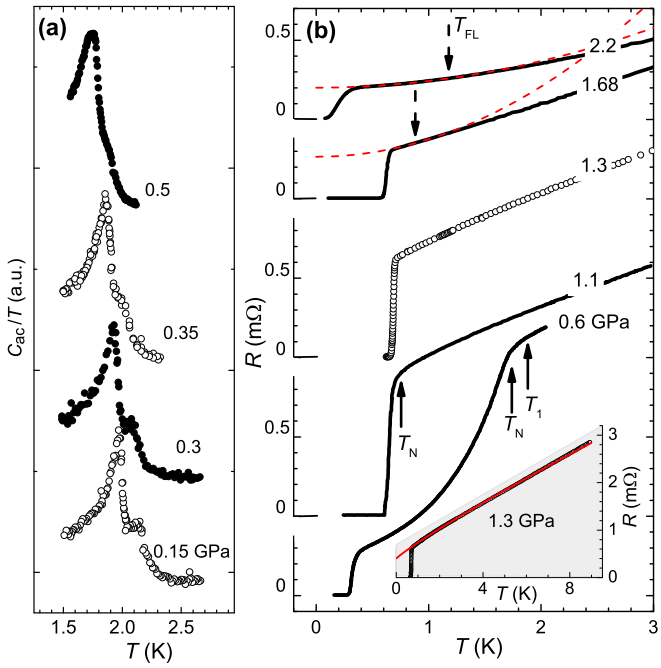

FIG. 4. (Color online) Experiments under hydrostatic pressure. (a) Results of ac calorimetry C_{ac} plotted in various applied pressures. For a better view data has been shifted along the C_{ac}/T axis. (b) Resistance R vs T for some selected pressures. Solid arrows show the magnetic transitions. Dashed arrows mark the upper limit (T_{FL}) of the $R(T) = R_0 + AT^2$ fits (red dashed lines). Inset: $R(T)$ at p_c in extended T range with fit (red line).

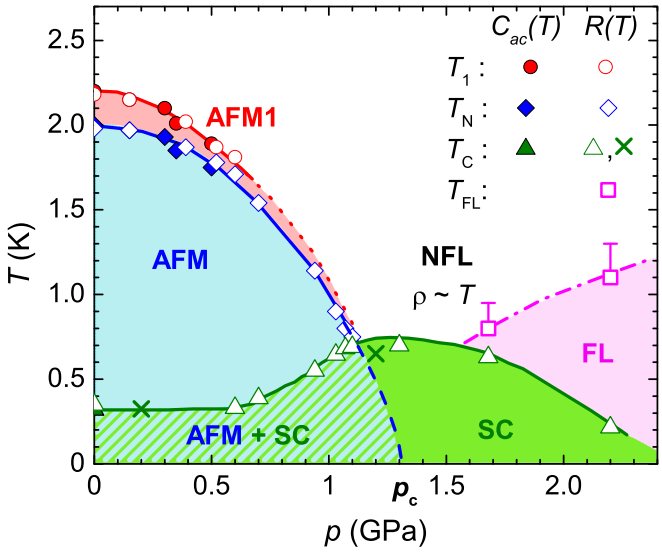

FIG. 5. (Color online) The zero field p-T phase diagram of Ce_3PtIn_{11}. Transition temperatures T_1 (circles), T_N (diamonds), T_c (triangles) and T_{FL} (squares) obtained from C_{ac} and R are denoted by closed and open symbols, respectively. The crosses are results from a sample from different batch. A possible continuation of $T_1 \to T_c$ ($T_N \to 0$) is indicated by the red dotted (blue dashed) line. The shaded area marks coexistence of SC and AFM. A purely SC ground state is found for $p > p_c$.

our present data an AFM spin-density wave type of QCP which predicts $R(T) \propto T^{d/z}$, where the dynamical exponent $z = 2$ and d is the effective dimensionality of the critical spin fluctuation [20], cannot be excluded. For pressures higher than $p > 1.68$ GPa we find that SC emerges out of a Fermi-liquid (FL) phase.

A possible scenario for understanding the properties of Ce_3PtIn_{11} can be preformed when taking some specific features of the crystal structure into consideration (3 Ce atoms/f.u. : 2Ce1 + 1Ce2). Because of the $CeIn_3$-like environment of the Ce2 site one might assume that the Ce2 sublattice orders AFM while the Ce1 sublattice, which is characterized by a "Ce_2PtIn_8" surrounding, is fully Kondo compensated. Consequently, the heavy QPs associated with the Ce1 sublattice take part in the SC condensate. Supports for this scenario might be found in thermodynamics. In the following we perform a crude analysis of our specific heat data based on two independent Ce sublattices despite the fact that this is not justified by the theory [8]. We postulate that $\gamma_0 = 0.52$ J/(mol K^2) from the Debye fit is associated with the Ce1 sublattice and subtract this term from the total electronic specific heat to obtain the Ce2-sublattice contribution, i.e., $C_{Ce2}/T = C_{el}/T - \gamma_0$. Figure 2 displays the corresponding entropies of both sublattices. As can be seen, the entropy of the Ce2 sublattice, S_{Ce2}, liberated at T_1, is found to be $0.5R \ln 2$ indicating that the ordered moment is lowered by Kondo interactions. The corresponding sublattice Kondo temperature is $T_{K2} \simeq 3$ K ($S_{Ce2} = 0.65R \ln 2$) [21]. The large S_{Ce2} below T_1 as well as the fact that T_{K2} is of the same order of magnitude as T_1 would suggest the presence of local moments. According to our postulate, C_{Ce1}/T gives a constant contribution over the entire T range ($0 < T < 30$ K). Such is unphysical, however the constant temperature dependence might approximate the HF behavior in the low-T region well. The associated entropy of the Ce1 sublattice, S_{Ce1}, is depicted in Fig. 2. T_{K1} equals 15 K which is of the same order as that found in Ce_2PdIn_8 ($T_K = 10$ K) [22]. Recognizing the assumption that the Ce1 sublattice is responsible for SC would imply that the normal state specific heat coefficient is not γ_n as it contains a contribution from the Ce2 sublattice but equals γ_0. Hence one obtains a value of $\Delta C/(\gamma_n T_c) \approx 1.6$, in fair agreement with the BCS value. This would support the coexistence of AFM and SC in a large part of the p-T phase diagram (see Fig. 5) as a consequence of a different ground state of each sublattice.

In summary, Ce_3PtIn_{11} is a heavy-fermion compound exhibiting two magnetic transitions at $T_1 \simeq 2.2$ K and $T_N \simeq 2.0$ K and a superconducting one at $T_c \simeq 0.32$ K at ambient pressure. Both the AFM order and SC coexist in a large region of the p-T phase diagram up to $p_c \simeq 1.3$ GPa, the compound's magnetic QCP. While still speculative, the QCP is of local-moment type. We suggest that the observed unusual properties can be related to the fact that Ce_3PtIn_{11} possesses two inequivalent Ce sites with distinctly different Kondo scales. However, the present state of knowledge of this new and interesting compound allowed us to perform only simple data analysis in terms of two independent Ce sublattices. Microscopic experiments (neutron scattering, NQR and NMR) are highly desirable to obtain relevant information on the coupling mechanism between the two Ce sublattices and thereby provide the basis for the theoretical description.

We would like to thank M. M. Abd-Elmeguid for critical reading of the manuscript and J. G. Sereni for helpful discussions. This work was supported by the Grant Agency of the Czech Science Foundation (Project No. P203/12/1201). Experiments were performed in MLTL (http://mltl.eu/) which is supported within the program of Czech Research Infrastructures (Project No. LM2011025).

[1] See for example: P. Gegenwart, Q. Si, and F. Steglich, Nat. Phys. **4**, 186 (2008), and references therein.

[2] P. Monthoux, D. Pines, and G. G. Lonzarich, Nature (London) **450**, 1177 (2007).

[3] C. Pfleiderer, Rev. Mod. Phys. **81**, 1551 (2009).

[4] A. M. Strydom, A. Pikul, F. Steglich, and S. Paschen, J. Phys.: Conf. Series **51**, 239 (2006).

[5] T. Goto, T. Watanabe, S. Tsuduku, H. Kobayashi, Y. Nemoto, T. Yanagisawa, M. Akatsu, G. Ano, O. Suzuki, N. Takeda, A. Dönni, and H. Kitazawa, J. Phys. Soc. Jpn. **78**, 024716 (2009).

[6] H. Mitamura, T. Tayama, T. Sakakibara, S. Tsuduku, G. Ano, I. Ishiti, M. Akatsu, Y. Nemoto, T. Goto, A. Kikkawa, and H. Kitazawa, J. Phys. Soc. Jpn. **79**, 074712 (2010).

[7] J. Custers, K.-A. Lorenzer, M. Müller, A. Prokofiev, A. Sidorenko, H. Winkler, A. M. Strydom, Y. Shimura, T. Sakakibara, R. Yu, Q. Si, and S. Paschen, Nat. Mater. **11**, 189 (2012).

[8] A. Benlagra, L. Fritz, and M. Vojta, Phys. Rev. B **84**, 075126 (2011).

[9] J. G. Sereni, O. Trovarelli, J. P. Kappler, C. Paschke, T. Trappmann, and H. v. Löhneysen, Physica B **199-200**, 567 (1994).

[10] J. D. Thompson and Z. Fisk, J. Phys. Soc. Jpn. **81**, 011002 (2012).

[11] J. D. Thompson, M. Nicklas, A. Bianchi, R. Movshovich, A. Llobet, W. Bao, A. Malinowski, M. F. Hundley, N. O. Moreno, P. G. Pagliuso, J. L. Sarrao, S. Nakatsuji, Z. Fisk, R. Borth, E. Lengyel, N. Oeschler, G. Sparn, and F. Steglich, Physica B **329-333**, 446 (2003).

[12] M. Kratochvílová, M. Dušek, K. Uhlířová, A. Rudajevová, J. Prokleška, B. Vondráčková, J. Custers, and V. Sechovský, J. Cryst. Growth **397**, 47 (2014).

[13] M. E. Fisher, Phil. Mag. **7**, 1731 (1962).

[14] H. Hegger, C. Petrovic, E. G. Moshopoulou, M. F. Hundley, J. L. Sarrao, Z. Fisk, and J. D. Thompson, Phys. Rev. Lett. **84**, 4986 (2000).

[15] M. B. Maple, J. W. Chen, Y. Dalichaouch, T. Kohara, C. Rossel, M. S. Torikachvili, M. W. McElfresh, and J. D. Thompson, Phys. Rev. Lett. **56**, 185 (1986).

[16] J. Van Kranendonk and J. H. Van Vleck, Rev. Mod. Phys. **30**, 1 (1958).

[17] P. Monthoux and G. G. Lonzarich, Phys. Rev. B **59**, 14598 (1999).

[18] T. Muramatsu, N. Tateiwa, T. C. Kobayashi, K. Shimizu, K. Amaya, D. Aoki, H. Shishido, Y. Haga, and Y. Ōnuki, J. Phys. Soc. Jpn. **70**, 3362 (2001).

[19] M. Nicklas, V. A. Sidorov, H. A. Borges, P. G. Pagliuso, C. Petrovic, Z. Fisk, J. L. Sarrao, and J. D. Thompson, Phys. Rev. B **67**, 020506(R) (2003).

[20] A. J. Millis, Phys. Rev. B **48**, 7183 (1993).

[21] H. Desgranges and K. Schotte, Phys. Lett. A **91**, 240 (1982).

[22] D. Kaczorowski, A. Pikul, B. Belan, L. Sojka, and Ya. Kalychak, Physica B **404**, 2975 (2009).